Classification of Dielectric Microparticles by Microwave Impedance Cytometry

Authors
Burak Sari[1]†, Uzay Tefek[2,3]†, M. Selim Hanay[2,3,*]

Affiliations

[1] Department of Electrical Engineering, Sabanci University, Istanbul 34956, TURKEY.

[2] Department of Mechanical Engineering, Bilkent University, Ankara 06800, TURKEY.

[3] UNAM – Institute of Materials Science and Nanotechnology, Bilkent University 06800, Ankara 06800, TURKEY

† These authors contributed equally to this work.
* Corresponding author, email: selimhanay@bilkent.edu.tr

Abstract

Coulter counters and impedance cytometry are commonly used for counting microscopic objects, such as cells and microparticles flowing in a liquid, as well as to obtain their size distribution. However, the ability of these techniques to provide *simultaneous material information* — via dielectric permittivity measurements — has been limited so far. The challenge stems from the fact that the signals generated by microparticles of identical size, but different material composition, are close to each other. The similarity in impedance signals arises because the material-dependent factor is determined mainly by the volume of aqueous solution displaced by the microparticles, rather than the microparticles themselves. To differentiate between materially distinct particles with similar geometry and size, another measurement mode needs to be implemented. Here, we describe a new microfluidics-based sensor that provides material classification between microparticles with similar sizes by integrating impedance cytometry with microwave resonator sensors on the same chip. While low-frequency impedance cytometry provides the geometric size of particles, the microwave sensor operating at three orders-of-magnitude higher frequency provides their electrical size. By combining these two measurements, the Clausius-Mossotti factors of microparticles can be calculated to serve as a differentiation parameter. In addition to distinguishing dielectric materials from cells and metals, we classified two different dielectric microparticles with similar sizes and electrical characteristics: polystyrene and soda lime glass, with 94% identification accuracy. The proposed

technique can serve as an automated monitoring system for quality control of manufactured microparticles and facilitate environmental microplastic screening.

Keywords: Impedance Cytometry, Microwave Sensors, Microplastics, Microparticles, Dielectric Characterization, Microwave Resonators, Split-Ring Resonators

Introduction

The characterization of microscale objects constitutes an important problem in biological, materials and environmental sciences. In biology, high-throughput techniques are needed to differentiate cell types[1] or test antibiotic susceptibility.[2] In materials science, the optimization of industrial microplastics, such as drug loading efficiency of micropolymers,[3] can increase the efficiency of medications, and lower their cost of production. In environmental screening, the widespread usage and high mobility of industrial microparticles have recently raised concerns about their environmental impact[4] especially within the context of microplastics pollution.[5] Some analytical techniques, such as Raman and Fourier Transform Infrared Spectroscopy (FTIR), are used for the material identification of microscale objects. Even though these techniques can provide accurate material characterization, they are regarded as expensive, non-portable, and time-consuming for microparticle analysis.[6,7] On the other hand, there are high-throughput techniques, such as Coulter counters[8] and impedance cytometry,[9] which provide the size of microparticles, but not their material type. By providing impedance cytometry with the capability for simple material characterization, the applications mentioned above can be facilitated much more rapidly. For instance, the elimination of a subset of microparticles early on from downstream analysis could possibly reduce the long analysis durations in microplastic workflows.

In impedance cytometry, cells and microparticles are detected via the changes in the ionic current as analyte particles pass through the proximity of the sensing electrodes. At low frequencies (<1 MHz, typically), a dielectric particle appears to be an ideal insulator as it blocks the ionic current. The blockage current is proportional to the volume of the particle, providing the means for sizing microparticles. At radio frequencies (typically 1 to 50 MHz in practice), the capacitive response of the dielectric particle starts to contribute to the impedance signal providing a potential route for material characterization. Indeed, many approaches in recent years

utilized the combination of a low-frequency (~1 MHz) and high-frequency (~50 MHz) simultaneous impedance sensing to differentiate non-biological microparticles (e.g. polystyrene microparticles) from biological cells.[2,10-15] In most of these studies, however, the differentiation was facilitated by the primarily water-based content of cells. The special role of water in impedance cytometry stems from the fact that water has a very large dielectric constant (ε_r=78 at 1 MHz) causing the impedance signals to strongly depend on the amount of water in a particle. As a result, the high-water content of biological particles, such as cells and pollen, renders them readily distinguishable from any other non-biological particles that lack water. The accuracy suffers when particles that do not contain water are to be differentiated. Since in this case, the impedance signal intensities they generate are predominantly determined by the aqueous solution they replace, rather than their intrinsic material properties (as discussed in the Theory section below).

While impedance cytometry took root in the last two decades for geometric sizing of particles, another electronic technique was being developed in parallel for microparticle analysis: microwave resonant sensors.[16-26] By operating at the GHz frequency range, these sensors can bypass the Debye screening effects and directly probe the capacitance of microparticles. The capacitance of this circuit is suddenly changed when a particle passes through the active sensing region, where an intense electrical field is present across two narrow electrodes. The modulation in the capacitance can be detected in the phase/amplitude response of the microwave resonator.

To overcome the challenge of differentiating non-biological microparticles in a potentially low-cost and high-throughput system, we combined two different electronic sensors, operating at frequencies more than three orders-of-magnitude apart: a low frequency (~1 MHz) impedance cytometry sensor[2,27-29] and a high frequency (~5 GHz) microwave capacitance sensor (Figure 1). The vast frequency difference enables the two sensors to provide two parameters complementary to each other. The low frequency sensor detects the geometrical volume of the particle (and its height) within the channel;[11] whereas the microwave sensor[16-26] yields electrical size which is a function of the particle geometrical volume and the Clausius-Mossotti factor of the particle, a factor that depends on the particle's electrical permittivity and provides a means for material differentiation (since different materials will have different electrical permittivity levels under the same conditions). We tested the platform on two common classes of non-biological

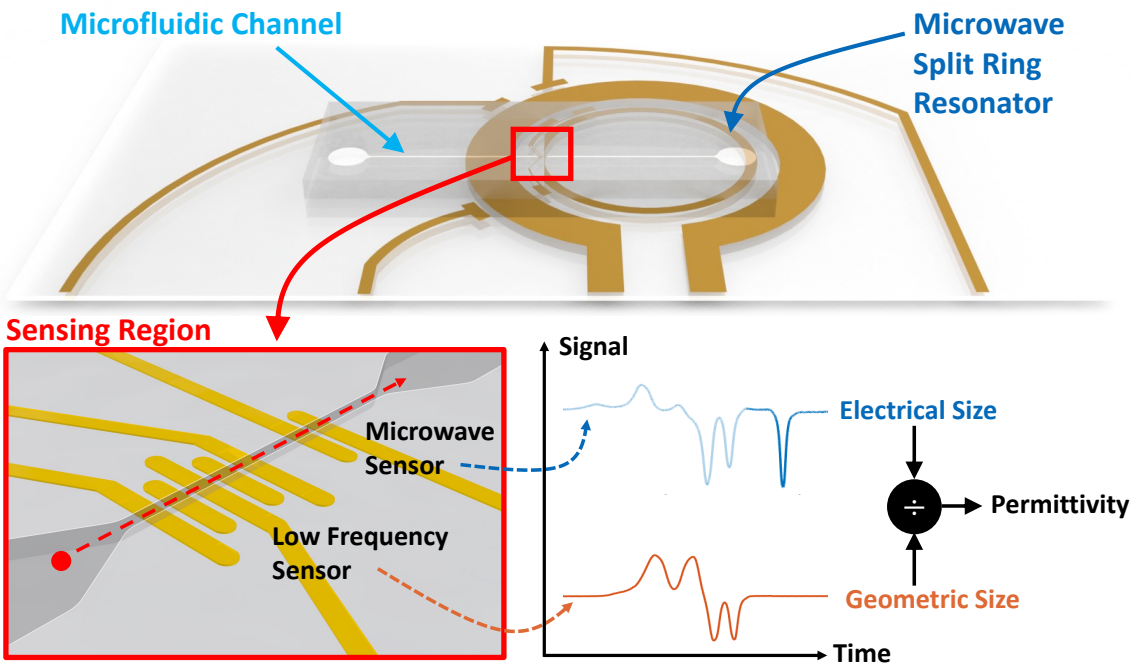

Figure 1: Sensing concept. On the microfluidic platform, there are two electronic sensors, a low frequency sensor with five electrodes and a microwave sensor (in the form of a split-ring resonator). As a particle passes through the sensing region, it induces signals that encode its geometric and electrical size (as well as the height of the particle in the channel, which is used for compensating positional dependency). By combining electrical and geometric size, the permittivity of each particle can be deduced.

microparticles approximately 20 μm in diameter: polystyrene (a typical microplastic) and soda lime glass (the most common household glass). Despite the low intrinsic contrast, our reported microfluidic sensor provided particle material identification with 94% accuracy.

Theory

The operation principles of both sensor technologies integrated here have been verified independently in earlier studies. For the low frequency sensor, the analyte particle induces an impedance change across a pair of electrodes in a conductive solution at 1 MHz. At low frequencies, a dielectric particle acts as an insulating object, partially blocking the ionic current between the electrodes. The amount of current blockade depends on particle's size (and position) in the channel, rather than its material properties such as permittivity.[8,9,30] Therefore, by

measuring the change in low frequency current passing through electrodes, one can obtain the geometric volume (V_p) of the particle: $\Delta I \propto V_p$.

The second measurement is the high-frequency (microwave) capacitance measurement ΔC which generates a signal[16-19] proportional to the multiplication of the volume of the particle and its Clausius-Mossotti factor (K_{CM}), $\Delta C \propto V_p \times K_{CM}$. K_{CM} is defined as:

$$K_{cm} \equiv \frac{\epsilon_p - \epsilon_m}{\epsilon_p + 2\epsilon_m} \quad (1)$$

where ε_p stands for the permittivity of the particle, and ε_m that of medium. By taking the ratio of the microwave signal (ΔC) to the low frequency signal (ΔI), we obtain a quantity that depends on the Clausius-Mossotti factor of a particle, but not its volume:

$$\frac{\Delta C\ (Microwave)}{\Delta I\ (1\ MHz)} \propto \frac{V_p\ \times K_{CM}}{V_p} = K_{CM} \quad (2)$$

Once K_{CM} is obtained, the permittivity of the particle can be back calculated by using the known value of the medium.

In the determination of the microwave capacitance change ΔC, the large dielectric constant of water smoothens out the differences in the response of different particles. As an example, consider the two classes of materials investigated in this work: polystyrene ($\varepsilon_r \sim 2.5$) and soda lime glass ($\varepsilon_r \sim 7.5$). While the ratio of their permittivity values is 3, this apparently large ratio does not show up in the magnitude of impedance signals. Rather, the measured signals mostly reflect the dielectric properties of the equivalent volume of water that each particle replaces in the sensing region, as dictated by the large permittivity of the medium (ε_m) in the Clausius-Mossotti formula (Equation 1). When the medium is water, the Clausius-Mossotti factors turn out to be -0.48 for polystyrene and -0.43 for soda lime glass: two close values differing by a fraction.

To put this in perspective, it is instructive to conduct a similar comparison for the differentiation of cells from microplastics. The relative permittivity values of cells range between 40-60;[31,32]

taking $\varepsilon_{r,cell}$ = 50 for concreteness, the Clausius-Mossotti value turns out to be -0.1 for a cell. This value is almost five times smaller than the K_{CM} of polystyrene. In other words, a polystyrene particle induces approximately five times larger signal compared to a single cell of similar size; but only a slightly larger signal compared to a microglass particle of similar size. Such small differences between the Clausius-Mossotti factors creates a challenge for the use of impedance cytometry in environmental screening to differentiate *non-biological microparticles from other types of non-biological particles* (*e.g.,* plastics *versus* glass particles). To overcome this challenge, we integrated two electronic sensor measurements, which operate at frequencies separated by three orders of magnitude (MHz *vs.* GHz).

Experimental Procedure

Standard microfabrication and soft lithography techniques were used to fabricate a glass/PDMS microfluidic system with a gold layer serving as the electrodes for both the low frequency and microwave sensors. The fabricated device (Fig. 2a) contains a microfluidic channel for analyte transportation, three gold tracks as the electrical ports of the low frequency sensor, and one SMA connector for microwave sensing. The two concentric circles visible in the picture form the microwave resonator, called a split ring resonator (SRR) explained in more detail below.[23,33,34] The sensing part of the device consists of two adjacent regions as shown in Figure 2b: 1) five consecutive electrodes for low-frequency measurements where the geometric size and height values of particles are obtained, 2) two microwave electrodes used for electrical volume measurements (they form a gap in the inner circle of the split ring resonator). Optical microscopy was used to observe the passage of particles through the sensing region concurrently with electronic measurements. For the analyte transportation, we used a PDMS microchannel which was sealed by the sensor chip. The microchannel was pressurized by Fluigent MFCS-EZ pressure control system and the analyte particles were passed through a constriction where all the electrodes were placed. The purpose of the constriction was to enhance the resolution of the current measurement signal and to reduce the passage of multiple particles simultaneously from the sensing region. The dimensions of the constriction were 60 μm in width and 45 μm in height. The flow rates through the constriction ranged from 2.4 μL/min to 4.8 μL/min. Particles typically passed through the sensing region within a duration of 20 ms each.

The low frequency part of the sensor closely follows the recent work [2,27-29]. Here, a five-electrode arrangement was used to obtain the geometric size of the particles while calibrating for the effect of height variation of particles as they flow through the channel (Figure 2 b,c). In the five-electrode arrangement, the 3rd electrode is used to provide a 1 MHz AC excitation voltage while the 1st and 5th electrodes are used to collect the resulting differential current. This current is carried by the ions in the solution, and a non-conducting particle passing through the channel blocks the ionic motion, resulting in a drop in the current proportional to the particle's volume. The remaining two electrodes, electrode 2 and 4, were kept floating: they were used to facilitate the height measurements by modifying the electric field between the middle and outer electrodes. A particle passing near the bottom of the channel induces a large variation in the current along its trajectory, whereas the current waveform is smoother for an identical particle passing near the top of the channel (Supplementary Figure 1) [2,27-29]. This way, the variation in the current for each trajectory was encoded by the ratio between the large and small peaks in the signal waveform (Figure 2d). This ratio, prominence (P), was then used to calculate the height of each particle and calibrate its response to obtain the geometric size accurately.

For the size and height measurement by the low frequency sensor, the 3rd electrode is driven by a 1 V peak-to-peak signal at 1 MHz from a lock-in amplifier (Zurich Instruments, HF2LI) and the resulting current is collected from the outer electrodes by a differential readout configuration. The current signals were converted into voltage by a transimpedance amplifier (Zurich Instruments, HF2TA), and read out by a lock-in amplifier (Zurich Instruments, HF2LI) in differential mode.

For electrical volume measurements at microwave frequencies, we used a split ring resonator [33,34] (SRR) which consists of two concentric rings. The microwave signal was fed through the outer ring which inductively excites the inner one. Since there was a split (a gap) along the inner ring, a standing-wave mode shape emerges and creates a high intensity electric field in the split region. [33,34] To increase the signal generated by the target particles, the width of the split gap was chosen to be 20 μm.

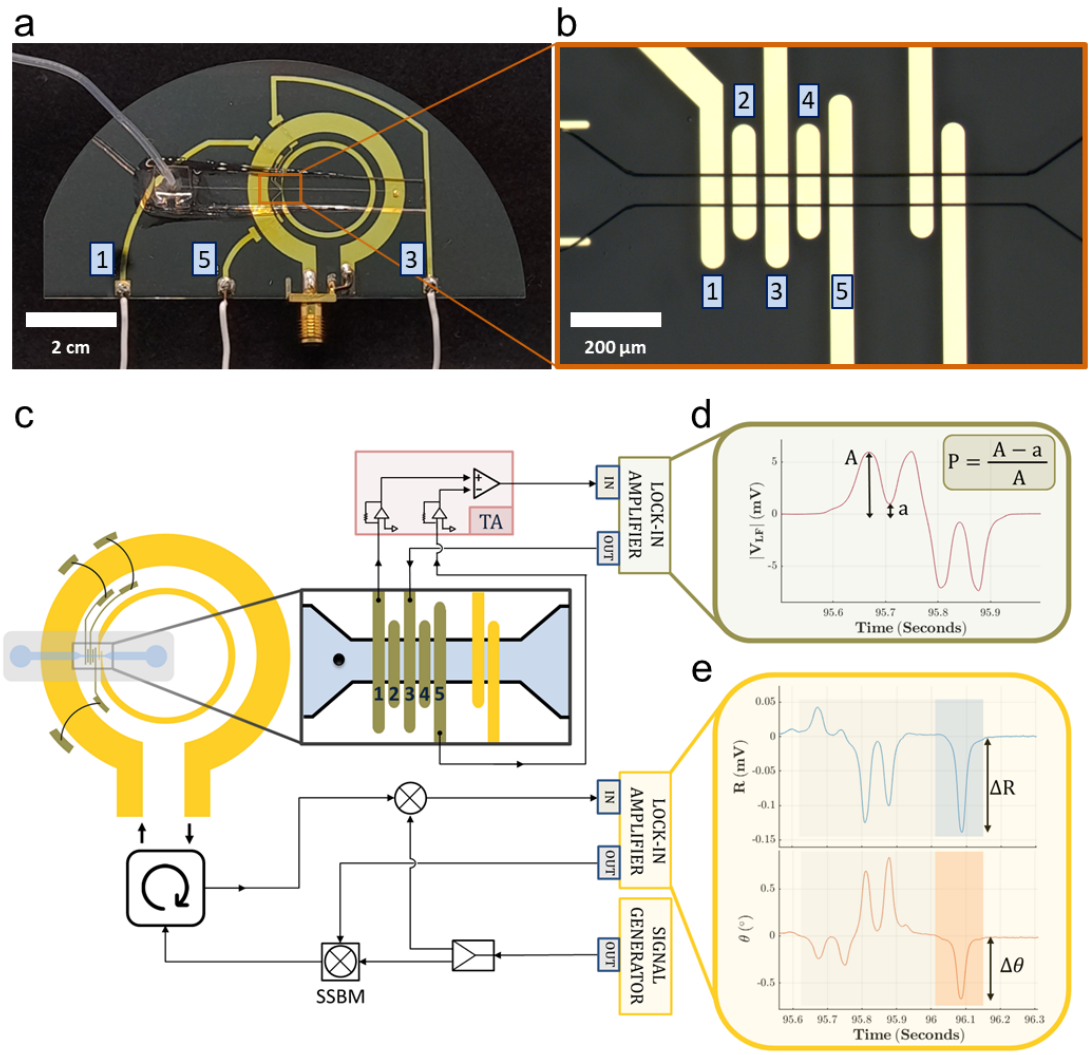

Figure 2: (a) A photograph of the sensor depicts: the microfluidic channel, the split ring resonator for microwave sensor terminated by an SMA connector, and three gold tracks for the low frequency sensor which are wire bonded to the pads to pass over the rings of the SRR. (b) A micrograph of the sensing region. The electrodes 1-3-5 are connected to the corresponding tracks in part (a). The low frequency excitation is provided from the 3rd electrode and collected from the 1st and 5th electrodes. The 2nd and 4th electrodes are kept floating to facilitate height measurements. The right two electrodes are for high frequency (microwave) measurements. (c) Simplified schematic of the circuit, SSBM: single side-band modulator, TA: Transimpedance Analyzer. (d) Low frequency current signal of a passing particle forms a bipolar Gaussian shape. The geometric size and height values of the particles are calculated from this measurement. (e) Microwave signals induced by a passing particle. The change in amplitude (R) and phase (θ) values in the highlighted sections are used to calculate the capacitance change induced by the particle.

After verifying the resonance characteristics of the SRR with a vector network analyzer (VNA), we switched to our custom circuitry (Figure 2c) and set the frequency of the signal generator to the resonance frequency (~5.4 GHz). The circuit consists of two lock-in amplifiers to employ single side band modulation (SSBM) and a signal generator as signal sources. We fed the SRR at its resonance frequency with 500mVpk power output. The time constant of the lock-in amplifiers was set to 501 μs and sampling rate were 13.39k/sec to fully detect rapidly passing particles. Since the maximum operational frequency of the lock-in amplifiers were below the resonance frequency, we built a custom Single Side Band (SSB) heterodyne circuitry[16,17] (Supplementary Figure S2). The reference signal outputs of the lock-in amplifiers were up-converted before entering the resonator and down-converted back before digitally reading the amplitude and phase of the signal. A detailed explanation of the circuitry can be found in the Supplementary Information Section 1.

Data Analysis

In experiments we recorded both the changes in low frequency (LF) current and high frequency (HF) reflected voltage wave. Subsequently, to analyze the data, we first start with analysis of the low frequency signal. The bipolar double gaussian form of the low frequency signal allows us to find and extract features of each event. To that end, we employ a similar algorithm used in.[27] In this algorithm odd-symmetric property of signal shape is exploited in the raw signal (Figure 3a).

The specific signal waveform created by particles in low frequency measurement was first used to find the location of each event in the raw data. Next the size and height information of each particle were extracted by using a fitting function on the detected events. Using the parameters outputted by this fitting (i.e. A, σ, γ in Figure 3b), the apparent diameter of the particle (before height compensation) and the prominence (which encodes the height information) were calculated. For the apparent diameter D, the signal depends on the maximum signal height, $A := G\sqrt[3]{A}$. Here G is a calibration constant of the circuitry, which can be determined with the help of a calibration particle whose precise diameter is known. In our circuitry, this constant was empirically found to be $385\ \frac{\mu m}{\sqrt[3]{Volts}}$. After the diameter calculation, the prominence was calculated by the form of double Gaussian formula ($P = 1 - 2e^{\frac{\gamma^2}{8\sigma^2}}$). The prominence parameter was then used to compensate for the travelling height of the particle by:

$$D_{compensated} = \frac{D}{c_1 P^2 + c_2 P + c_3} \quad (3)$$

The determination protocol for constants (i.e., c_1, c_2, c_3) are explained in detail in SI Section 3.

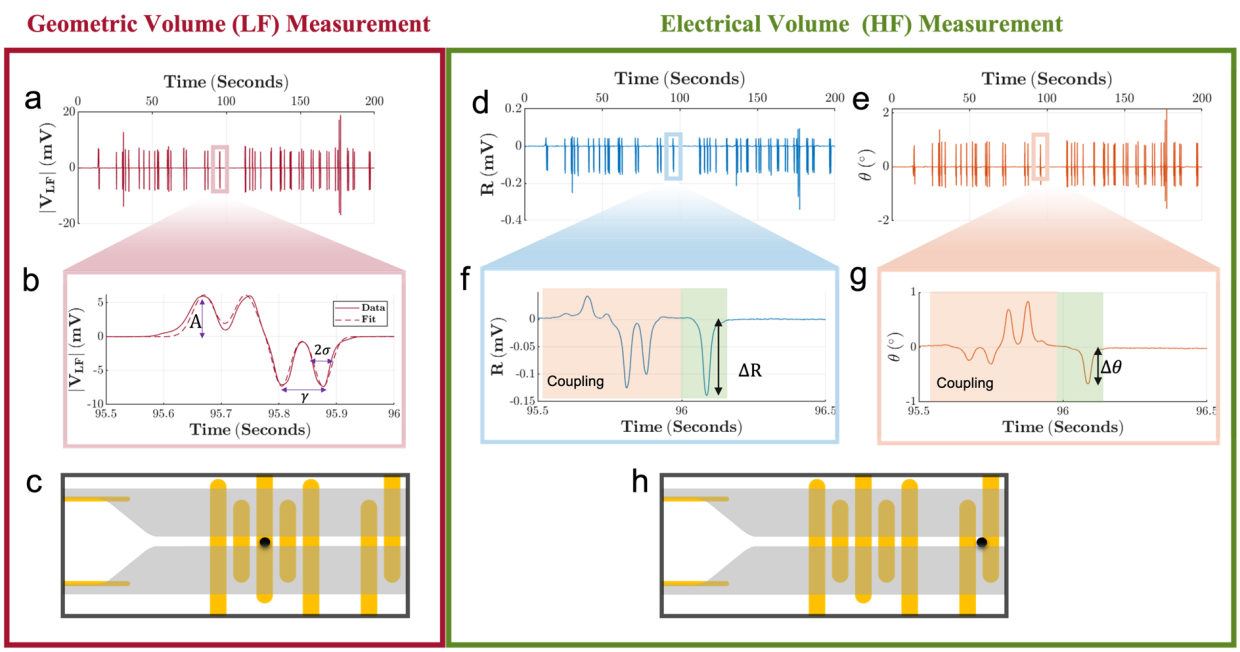

Figure 3: (a) Time-domain data of low frequency (LF) measurement in a typical run, (b) shows time domain data of single event along with fitting (dashed) that is used to extract features, (c) shows particle's position schematically while the LF signal is recorded, (d-e) show raw time domain data of high frequency (HF) amplitude and phase measurement, (f-g) show time domain data of single event along with measurement parameters. The signal annotated as coupling emerges when the particle is still in the low-frequency measurement region and is not used for electrical volume measurements. Rather, signals denoted as ΔR and $\Delta\theta$ which emerge when the particle is between the split-ring region are used. (h) Shows particle position while HF signals are recorded.

After the low frequency sensor, we then analyzed the signal from the microwave sensor. Here, the induced capacitance change, ΔC by the particle is formulated as [16,17]:

$$\Delta C = \epsilon_m V_p K_{CM} \frac{|E_{RMS}|^2}{U_{RMS}^2} \quad (4)$$

where E_{RMS} denote the root-mean-squared (rms) Electric Field at the location of the particle, and U_{RMS} designate the rms voltage difference in the microwave sensor. To obtain the capacitance change, we monitor the amplitude (R) and phase (θ) response of the microwave resonator to calculate the out-of-phase component (Y quadrature, $Y \equiv R\ sin\theta$) of the reflected voltage from the microwave resonator (Fig. 3d-e). Any fractional change in the capacitance of the microwave resonator is reflected in the out-of-phase component (Supplementary Information Section 2):

$$\Delta Y \propto \frac{\Delta C}{C} \quad (5)$$

Here, ΔY denotes the change in the out-of-phase component of the reflected voltage, and C denotes the total capacitance of the microwave resonator.

Due to the close placement of the microwave electrodes with respect to the low frequency electrodes, data analysis of microwave amplitude and phase signals is greatly simplified. Low frequency and high frequency measurements are synchronous; the double gaussian form of LF signal corresponds to orange shaded regions in Fig. 3f-g in terms of timing. By using the knowledge of the position and length of the double Gaussian waveform in time, a script automatically determined the peaks and dips in microwave domain after the orange shaded region to extract ΔR and $\Delta\theta$ values of each event (Figure 3f-g). By using these two parameters, the capacitance change induced by a particle can be calculated by the relationship: $\Delta Y = \Delta R \sin(\theta) + R\cos(\theta)\Delta\theta$ where R and θ correspond to baseline value of raw signals. We define ΔY as the *electrical volume* and $\sqrt[3]{\Delta Y}$ as the *electrical diameter*. To compensate for the height, we use the same parameters extracted from the LF measurements:

$$Electrical\ Diameter_{compensated} = \frac{\sqrt[3]{\Delta Y}}{c_1 P^2 + c_2 P + c_3} \quad (6)$$

This way, the two-sensor system provides the height-compensated values for both geometric diameter (eqn. 3) and the electric diameter (eqn. 6) which can be used for material classification. Since the same constants are used in the compensation protocols in equations (3) and (6), the separability of the different materials is not affected by this procedure.

Results

With this analysis procedure we compared the measurements from two types of microparticles, polystyrene and soda lime glass. On Figure 4a, we charted the LF measurements *vs*. the microwave measurements. The slope on this chart is proportional to the K_{CM} value for each particle: indeed, the separation of the slopes of the two datasets is evident, especially in the zoomed in version, Figure 4b. As expected, polystyrene particles have higher $|K_{CM}|$ and this fact is reflected in Figure 4a-b as they have a sharper slope compared to soda lime glass ($|K_{CM}|$ factors of polystyrene and soda lime glass are 0.48 and 0.43, respectively). When we consider the expressions for geometric diameter (eqn. 3) and electric diameter (eqn. 6), their ratio corresponds to the cube root of their K_{CM} values.

$$\frac{Electrical\ D}{Geometric\ D} = \frac{\sqrt[3]{\Delta Y}}{G\sqrt[3]{a}} \approx \sqrt[3]{K_{CM}} \quad (7)$$

Indeed, the ratio of the slopes in the fit lines in Fig. 4a follow the expected value from the nominal values of the permittivity (1.03 *vs.*1.16 respectively).

A salient feature of Fig. 4 (a,b) is that polystyrene has a narrower size distribution compared to soda lime glass particles. This observation agrees with the geometric size distribution given by the manufacturer of the microparticles. Polystyrene particles (Sigma-Aldrich,74491-10ML-F) are reported to have a size distribution of 20 ± 0.3 µm, whereas soda lime glass (Cospheric, SLGMS-2.5, 15-22 μm size distribution) is reported to have diameters changing in range of $15 - 22\ \mu m$. Therefore, it is expected that soda lime glass particle will have a much wider size distribution, as observed in Figure 4. The black line in Fig. 4b shows the separation region between the polystyrene and soda lime glass. Within this binary separation protocol, the technique achieves correct separation with 94.8% accuracy overall. Material specific misclassification rates are detailed in Table 1.

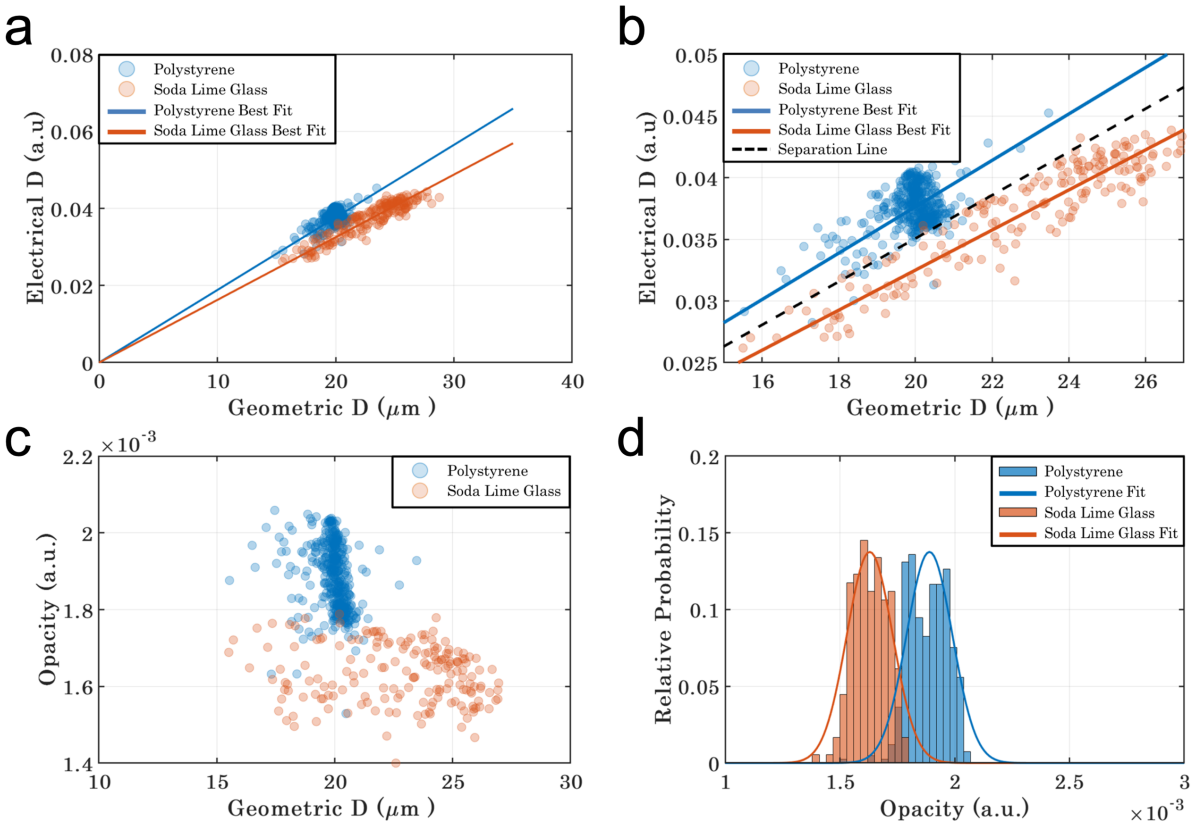

Figure 4: (a) Separation of polystyrene and soda lime glass using geometric and electrical diameter (b) Close up view of the separation interface (c) Separation by the microwave opacity of polystyrene and soda lime glass (d) histogram of opacity showing material classification along with separating Gaussian fits.

Fig. 4c shows the *opacity* of the particles at microwave frequencies which is a parameter used to determine the amount of electrical field penetration[2] a particle allows for. Within the proposed system, opacity is calculated as:

$$Opacity = \frac{Electrical\ D}{Geometric\ D} = \frac{HF\ Response}{LF\ Response} \quad (8)$$

It appears from the results that polystyrene beads are more opaque to electrical field penetration. This is indeed also expected because of the permittivity contrast with water. Whenever there is an interface in fluid where ions are present, these ions block the field penetration (i.e., Debye Screening). At microwave screening where Debye screening no longer effects signal magnitude, the opacity is seemingly proportional to the cube-root of Clausius-Mossotti factors. In this case,

the opacity values are 1.9 10^{-3} (σ =9.9 10^{-5}) for polystyrene and 1.7 10^{-3} (σ =1.1 10^{-4}) for soda lime glass. The histogram in Fig. 4d suggests that this opacity difference can be used to classify different dielectric materials. We also verify that the integrated approach presented here can readily differentiate a non-biological particle from a biological cell; or a dielectric microparticle from a metallic microparticle as shown in Fig. S5. This way, different classes of materials, in addition to different dielectric materials, can be quickly and reliably distinguished with this approach.

	Number of Particles	**Number of Misclassifications**	**Successful Separation (%)**
Polystyrene	412	17	95.8
Soda Lime Glass	167	13	92.2
Total	579	30	94.8

Table 1: Statistics of Analyzed and Classified Dielectric Microparticles

Conclusion

In conclusion, we have shown that two different classes of dielectric microparticles that have very similar electronic signatures can be differentiated from each other based on their permittivity. To achieve this distinctive capability, we integrated two different electronic sensors that operate at frequencies separated by three orders-of-magnitude: a 1 MHz sensor for geometric sizing and a microwave (~ 5 GHz) sensor for electrical sizing. By combining the two signals, we obtained an intrinsic material property for each microparticle and reached an identification accuracy of 94% in the binary classification of polystyrene and glass microparticles. A sensor with higher resolution can enable the differentiation of microparticles amongst a larger variety of material classes, which will be of immense benefit for the materials and environmental sciences and their applications.

Methods

The sensor device was fabricated on one half of a 100 mm x 0.5 mm (diameter x thickness) double-side polished wafer. The substrate was chosen to be dry fused quartz, a non-conductive and low loss-tangent material. Sensor geometry was patterned by spin coating 2 μm thick AZ –

5214 photoresist and photolithography steps. After the photoresist development in AZ – 400K for 30 seconds, 5 nm of chromium and 150 nm of gold were deposited by the thermal evaporation process. Chromium was used as a binding agent between quartz and gold layers. After an overnight acetone lift-off process, the sensor pattern was completed. For the microchannel fabrication, SU-8 mold was used to create channel patterns on a PDMS block. After punching the fluidic inlet and outlet through the PDMS block, the bottom surface of the channel and the gold deposited wafer was treated with oxygen plasma to activate their surfaces. Within ten minutes after the activation, the microfluidic channel and the wafer were aligned and bounded under an optic microscope.

To increase the magnitude of the current, and maintain compatibility for cell characterizations, we used 0.2% Tween 20 (Sigma-Aldrich, P1379-500ML) added Phosphate-buffered saline (Biowest, L0615-500) as the medium in the experiments which has a conductivity of 9 mS/cm. Polystyrene particles were received in DI water: a 5 µL volume of this solution was mixed with a 5 mL volume of the Tween 20 / PBS solutions. Soda lime glass particles were received as a solid powder and dissolved in the same Tween 20 / PBS solution. The two types of particles had similar diameters and optical appearances, making it difficult to identify them by optical microscopy at flow speeds used in the measurements. For this reason, particles were passed through the sensor system sequentially to have an independent verification of the identity of each particle. The microwave resonance curves were compared between the runs to ensure that device sensitivity was not changed. The tests were repeated on a second device with identical dimensions, and the separation between the two class of microparticles were verified with similar accuracy level.

Acknowledgements

The authors thank Hashim Alhmoud, Ceren Alatas, Berk Kucukoglu, Hadi S. Pisheh and Arda Secme for useful discussions. This project has received funding from the European Research Council (ERC) under the European Union's Horizon 2020 research and innovation programme (grant agreement No 758769)

References

1 Nagrath, S. *et al.* Isolation of rare circulating tumour cells in cancer patients by microchip technology. *Nature* **450**, 1235-1239 (2007).

2 Spencer, D. C. *et al.* A fast impedance-based antimicrobial susceptibility test. *Nature Communications* **11**, 1-11 (2020).

3 Lagreca, E. *et al.* Recent advances in the formulation of PLGA microparticles for controlled drug delivery. *Progress in Biomaterials* **9**, 153-174 (2020).

4 Bizmark, N., Schneider, J., Priestley, R. D. & Datta, S. S. Multiscale dynamics of colloidal deposition and erosion in porous media. *Science Advances* **6**, eabc2530 (2020).

5 Lim, X. Microplastics are everywhere—but are they harmful? , (Nature Publishing Group, 2021).

6 De Frond, H. *et al.* Monitoring microplastics in drinking water: An interlaboratory study to inform effective methods for quantifying and characterizing microplastics. *Chemosphere* **298**, 134282 (2022).

7 Blevins, M. G. *et al.* Field-Portable Microplastic Sensing in Aqueous Environments: A Perspective on Emerging Techniques. *Sensors* **21**, 3532 (2021).

8 Hogg, W. R. & Coulter, W. H. Apparatus and method for measuring a dividing particle size of a particulate system. US3557352 (1971).

9 Gawad, S., Schild, L. & Renaud, P. Micromachined impedance spectroscopy flow cytometer for cell analysis and particle sizing. *Lab on a Chip* **1**, 76-82 (2001).

10 Hoffman, R. & Britt, W. Flow-system measurement of cell impedance properties. *Journal of Histochemistry & Cytochemistry* **27**, 234-240 (1979).

11 Cheung, K., Gawad, S. & Renaud, P. Impedance spectroscopy flow cytometry: On-chip label-free cell differentiation. *Cytometry Part A* **65**, 124-132 (2005).

12 Sun, T., Bernabini, C. & Morgan, H. Single-colloidal particle impedance spectroscopy: Complete equivalent circuit analysis of polyelectrolyte microcapsules. *Langmuir* **26**, 3821-3828 (2010).

13 Clausen, C. H. *et al.* Bacteria detection and differentiation using impedance flow cytometry. *Sensors* **18**, 3496 (2018).

14 Sun, T. & Morgan, H. Single-cell microfluidic impedance cytometry: a review. *Microfluidics and Nanofluidics* **8**, 423-443 (2010).

15 Colson, B. C. & Michel, A. P. Flow-through quantification of microplastics using impedance spectroscopy. *ACS Sensors* **6**, 238-244 (2021).

16 Nikolic-Jaric, M. *et al.* Microwave frequency sensor for detection of biological cells in microfluidic channels. *Biomicrofluidics* **3**, 034103 (2009).

17 Ferrier, G. A., Romanuik, S. F., Thomson, D. J., Bridges, G. E. & Freeman, M. R. A microwave interferometric system for simultaneous actuation and detection of single biological cells. *Lab on a Chip* **9**, 3406-3412 (2009).

18 Afshar, S. *et al.* Multi-frequency DEP cytometer employing a microwave sensor for dielectric analysis of single cells. *IEEE Transactions on Microwave Theory and Techniques* **64**, 991-998 (2016).

19 Kelleci, M., Aydogmus, H., Aslanbas, L., Erbil, S. O. & Hanay, M. S. Towards microwave imaging of cells. *Lab on a Chip* **18**, 463-472 (2018).

20 Yang, Y. *et al.* Distinguishing the viability of a single yeast cell with an ultra-sensitive radio frequency sensor. *Lab on a Chip* **10**, 553-555 (2010).

21 Dalmay, C. *et al.* Ultra sensitive biosensor based on impedance spectroscopy at microwave frequencies for cell scale analysis. *Sensors and Actuators A: Physical* **162**, 189-197 (2010).

22 Chen, T. *et al.* in *2013 IEEE MTT-S International Microwave Symposium Digest (MTT).* 1-4 (IEEE).

23 Rowe, D. J. *et al.* Improved split-ring resonator for microfluidic sensing. *IEEE Transactions on Microwave Theory and Techniques* **62**, 689-699 (2014).

24 Ma, X., Du, X., Li, H., Cheng, X. & Hwang, J. C. Ultra-wideband impedance spectroscopy of a live biological cell. *IEEE Transactions on Microwave Theory and Techniques* **66**, 3690-3696 (2018).

25 Chien, J.-C. *et al.* A high-throughput flow cytometry-on-a-CMOS platform for single-cell dielectric spectroscopy at microwave frequencies. *Lab on a Chip* **18**, 2065-2076 (2018).

26 Watts, C. *et al.* Microwave Dielectric Sensing of Free-Flowing, Single, Living Cells in Aqueous Suspension. *IEEE Journal of Electromagnetics, RF and Microwaves in Medicine and Biology* (2019).

27 De Ninno, A. *et al.* Coplanar electrode microfluidic chip enabling accurate sheathless impedance cytometry. *Lab on a Chip* **17**, 1158-1166 (2017).

28 Spencer, D. & Morgan, H. High-speed single-cell dielectric spectroscopy. *ACS Sensors* **5**, 423-430 (2020).

29 Zhong, J., Liang, M. & Ai, Y. Submicron-precision particle characterization in microfluidic impedance cytometry with double differential electrodes. *Lab on a Chip* **21**, 2869-2880 (2021).

30 Fraikin, J.-L., Teesalu, T., McKenney, C. M., Ruoslahti, E. & Cleland, A. N. A high-throughput label-free nanoparticle analyser. *Nature Nanotechnology* **6**, 308-313 (2011).

31 Zedek, A., Dubuc, D. & Grenier, K. in *2017 IEEE MTT-S International Microwave Symposium (IMS).* 865-868 (IEEE).

32 Nerguizian, V., Alazzam, A., Stiharu, I. & Burnier Jr, M. Characterization of several cancer cell lines at microwave frequencies. *Measurement* **109**, 354-358 (2017).

33 Lee, H.-J. & Yook, J.-G. Biosensing using split-ring resonators at microwave regime. *Applied Physics Letters* **92**, 254103 (2008).

34 Salim, A. & Lim, S. Complementary split-ring resonator-loaded microfluidic ethanol chemical sensor. *Sensors* **16**, 1802 (2016).